

Jet Flow Structure under the Perturbation of Two Unsteady Microjets

P. Zhang¹ and Y. Zhou²

¹Department of Mechanical Engineering
 The Hong Kong Polytechnic University, Hong Kong SAR, China

²Institute for Turbulence-Noise-Vibration Interaction and Control
 Shenzhen Graduate School, Harbin Institute of Technology, Shenzhen, China

Abstract

The manipulation of turbulent jet mixing has great potential benefits in various industrial applications. This work reports an experimental investigation on the active control of a turbulent round air jet using two unsteady radial microjets. Two microjets were placed at diametrically opposite locations upstream of the nozzle exit. The Reynolds number was 8,000. The flow rate ratio C_m and excitation frequency ratio f_e/f_0 of the microjets to the main jet were varied over the ranges of 0 – 16% and 0 – 1.4, respectively, where f_e was the excitation frequency of unsteady microjets and f_0 the preferred-mode frequency in the uncontrolled jet. It has been found that, given $f_e/f_0 \approx 1$, jet mixing can be greatly improved with a small C_m . The flow physics is explored based on flow visualization technique in two orthogonal diametrical planes through the geometric axis of the flow, as well as a number of cross-sectional planes normal to the axis. It has been found that strong entrainment is predominant in the injection plane of microjets. In contrast, rapid spreading occurs in the orthogonal non-injection plane. A close examination of flow visualization photographs unveils that a number of structures are sequentially ‘tossed’ out along the radial direction in the non-injection plane, which is accompanied by a strong ejection of jet core fluid, often in the form of one pair of mushroom-like counter-rotating structures and one pair after another. The finding is distinct from previously reported changes in the flow structure under the manipulation of steady microjets, tabs and other techniques. A conceptual model of the flow structure under the excitation of two unsteady microjets is proposed for the first time.

Introduction

Understanding jet mixing is of fundamental and crucial importance to many engineering applications such as noise suppression, combustion, lift augmentation, heat transfer and chemical reactors. Naturally, its control for mixing enhancement has received a great deal of attention in literature. The concept to use control jets to enhance jet mixing was proposed by Davis [1]. Seidel et al. [7] emulated the performances of noncircular jets by placing around a round main jet multiple steady radial blowing jets at positions where the corners or vortices would be if noncircular nozzles were used. Their results agreed surprisingly well with those of corresponding noncircular jets [4], indicating that a jet may be controlled, based on fluidic means, to achieve the optimized performance under different operation conditions. Please refer to Henderson [2] for a recent review on the implementation of microjets for jet control.

This work is focused on the control of two unsteady microjets placed oppositely in a diametrical plane through the geometric axis of the nozzle prior to jet issuing. Two control parameters are examined in detail, i.e., the mass flow rate ratio C_m of microjets to the main jet and the frequency ratio f_e/f_0 , where f_e and f_0 are the excitation frequency and the preferred-mode frequency in the uncontrolled jet, respectively. Flow structures with and without

control are measured using flow visualization technique in order to gain a relatively thorough understanding of interactions between the main jet and unsteady microjet excitation.

Experimental Details

Experimental Setup

The experimental setup consists of the main jet and microjet assemblies. Figure 1(a) shows that, once entering a large mixing box, air is mixed with seeding particles when flow visualization measurement is conducted; it passes through a tube, a plenum box, a 300-mm-long diffuser of 15° half-angle and two fine screens before reaching a cylindrical settling chamber of 400 mm in length and 114 mm in diameter. The nozzle contraction follows a contour specified by equation $R = 57 - 47\sin^{1.5}(90^\circ - 9x/8)$, where x' axis (unit: mm) is attached to the nozzle centerline with x' equal to zero at nozzle exit and its positive direction toward nozzle entrance; the contraction ratio is 32.5 with an exit diameter D of 20 mm. The nozzle was extended by a 47-mm-long smooth circular passage of the same diameter D . The jet issues into an air-conditioned spacious laboratory. The exit Reynolds number $Re_D = U_e D / \nu$ of the main jet is fixed at 8000, where U_e is the centreline velocity in the exit plane and ν is kinematic viscosity.

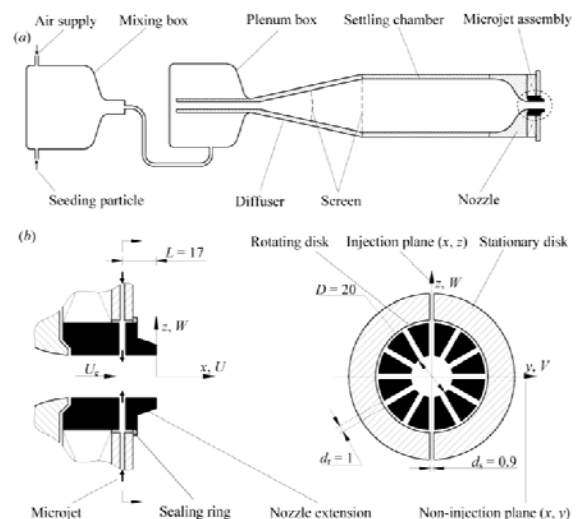


Figure 1. Schematic of experimental setup: (a) main-jet assembly; (b) microjet assembly.

The control jets are unsteady microjets. The microjet assembly (figure 1b) comprises a stationary and a rotating disk. The stationary disk is drilled with 6 orifices of 0.9 mm in diameter and distributed azimuthally at 60-deg interval. These orifices are connected through short and equal-length tubes to a chamber. The rotating disk is drilled with 12 orifices of 1 mm in diameter, azimuthally equally spaced, which are 17 mm upstream of the

exit. The rotating disk is the rotor of a servo motor with a maximum speed of $N = 2950 \text{ rpm}$. Once the orifices on the stationary and the rotating disks are aligned during rotation, a pulsed microjet is emitted towards the main jet axis as shown in figure 1(b). Two in-phased unsteady microjets were presently used to manipulate the main jet. The microjet excitation frequency f_e is then $12N/60$, corresponding to a frequency range of 0 to 590 Hz, well covering the preferred-mode frequency f_0 of 128 Hz in the uncontrolled jet. The flow rates of both main jet and control microjets are adjustable independently via two separate flowmeters, whose experimental uncertainty is no more than 1%.

The coordinate system is defined such that its origin is at the centre of the nozzle extension exit, with the x axis along the streamwise direction, the z axis along the radial microjet and the y axis along the direction normal to both x and y , following the right-hand system. The (x, z) and (x, y) planes are referred to as the injection and non-injection planes, respectively (figure 1b). Following Zhou *et al.* [9], the jet centerline decay rate K is used to evaluate main jet mixing, given by $(\overline{U}_e - \overline{U}_{5D})/\overline{U}_e$, where the overbar denotes time-averaging, \overline{U}_e and \overline{U}_{5D} are the time-averaged centerline velocities at $x/D = 0$ and 5, respectively.

Hotwire and Flow Visualization Techniques

A single tungsten wire of 5 μm in diameter, operated on a constant temperature circuit at an overheat ratio of 1.8, was used to measure the value of K . The signal from the wire was offset, filtered at a cut-off frequency of 2.8 kHz, amplified and then digitized using a 12-bit A/D board at a sampling frequency of 6 kHz. The duration for each record was 80 s. This hotwire probe was mounted on a computer-controlled two-dimensional traversing mechanism whose streamwise and transverse resolutions were both 0.01 mm.

A planar particle image velocimeter was used for flow visualization in the injection (x, z) plane and the non-injection (x, y) plane, as well as a number of cross-sectional (y, z) planes. A TSI oil droplet generator was used to generate fog for the seeding of flow visualization measurements. The fog particles, with a size of about 1 μm in diameter, were introduced into the upstream mixing chamber (figure 1a), thus homogeneously distributed throughout the main jet. The captured images covered an area of $x/D = 0 \sim 10$ and y/D or $z/D = -5 \sim +5$ in the (x, y) and (x, z) planes and an area of $y/D = -4 \sim +4$ and $z/D = -4 \sim +4$ in the (y, z) planes at $x/D = 0.7, 1.0, 1.3, 1.6, 2.0, 2.4, 2.7, 3.0, 4.0$ and 5.0.

Results

Dependence of Jet Decay Rate on C_m and f_e/f_0

The C_m was varied from 0.0% (no control) to 16% in order to determine its influence on jet mixing. Consider the case of $f_e/f_0 = 1.14$, that is, the excitation frequency is close to the preferred-mode frequency of the main jet. The K (figure 2a) exhibits a strong dependence on C_m . We may divide the dependence of K on C_m into three types, i.e., I ($C_m < 2.6\%$), II ($C_m = 2.6 - 4.5\%$), and III ($C_m > 4.5\%$). In Type I, K is highly sensitive to C_m , rising rapidly from 0.054 at $C_m = 0.0\%$ to about 0.2 at $C_m \approx 1.0\%$ and then dropping quickly until $C_m = 2.0\%$. In Type III, K increases steadily, albeit much less rapidly than in Type I, and appears approaching asymptotically to a constant. Type II where the distribution of K exhibits a minor hump and is apparently a transition between Types I and III. The three distinct behaviors of K suggest different flow physics or control mechanisms behind, as confirmed by Zhang *et al.* [8].

The dependence of K on f_e/f_0 is examined at $C_m = 1.5\%$, at which the maximum K occurs in Type I. As shown in figure 2(b), K is enhanced with increasing f_e/f_0 , reaching the maximum ($K = 0.215$) at $f_e/f_0 = 1.0$ before its approximately linear fall. A minor trough

occurs at $f_e/f_0 = 0.86$. In comparison, C_m required to achieve the same K value (0.215) is 4.5% given two steady microjets, three times that of the unsteady counterpart, demonstrating high control efficiency in the use of the unsteady microjet control.

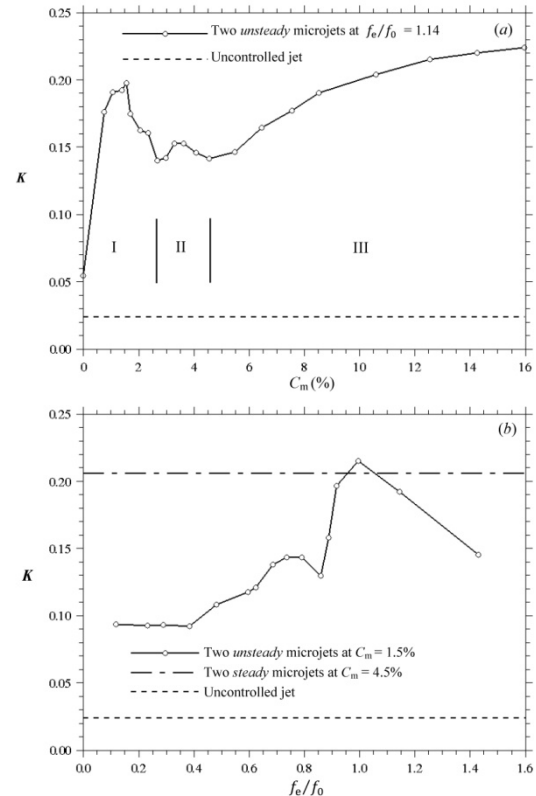


Figure 2. Dependence of the jet decay rate K on: (a) the mass flow ratio C_m ($f_e/f_0 = 1.14$); (b) the excitation frequency f_e/f_0 ($C_m = 1.5\%$).

Flow Structure Development under Control

Great attention was given to the three-dimensional flow structures in Type I, which is especially fascinating. In order to gain a relatively thorough understanding of the flow physics, flow visualization measurements were conducted in the (x, y) , (x, z) and (y, z) planes of Type I. Figure 3 presents typical photographs from flow visualization, taken in the (x, y) and (x, z) planes. For the purpose of comparison, the photographs taken in the uncontrolled jet (figure 3a) are also included in the figure. There is a profound change in the flow structure with and without control. For Type I ($f_e/f_0 = 1.0$ for $C_m = 1.5\%$), the shear layer rolls up early to form stronger vortices in both the (x, y) and (x, z) planes (figure 3b1 and 3b2) than the uncontrolled jet (figure 3a). Meanwhile, there is a distinct difference between the two planes of Type I. A large amount of ambient fluid (dark-colored) in the injection plane is engulfed vigorously into the jet even right near the jet axis via vortical motions. In contrast, smoke-marked fluid (white-colored) is rather massively ejected from the braid region between two successive vortices in the non-injection plane, generating a much extensive spread than the uncontrolled case.

Figure 4 presents typical photographs from flow visualization, taken in the cross-sectional plane of the controlled jet at $x/D = 0.7, 1.0$ and 1.3 (Type I: $f_e/f_0 = 1.0$ for $C_m = 1.6\%$), along with their counterparts without control. The natural jet images look like a full moon, suggesting no rollup motion. Once excited, the shear layer displays rollup motions at two different streamwise locations-between the injection and the non-injection planes. At $x/D = 0.7$, the shear layer rolls up early near the injection plane, generating two roll segments (figures 4b1 and 4b2). This is caused by a higher level of initial velocity fluctuation about the injection plane than about the non-injection plane. It has been noted that the two roll segments are symmetrical about a plane

through the jet axis, displaying an angle of roughly 15° with respect to the injection plane. Occurrence of the angle is linked to the azimuthal deflection of the initial shear layer along the exit perimeter under the influence of the rotating nozzle extension. Further downstream at $x/D = 1.0$, the shear layer rollup is also evident about the non-injection plane (figure 4c1). Figures 4(c1) and 4(c2) exhibit sequential images of two phases with time separation $450 \mu\text{s}$ in one period $T = 7812.5 \mu\text{s}$ (for $f_e/f_0 = 1$) of roll segments passing downstream. It has been found from the sequential images that the vortex segment near the non-injection plane moves downstream of that near the injection plane. Further, the two roll segments on each side of the injection plane join those near the non-injection plane, with the reoriented ends for each segment, forming a contorted ring structure (not shown).

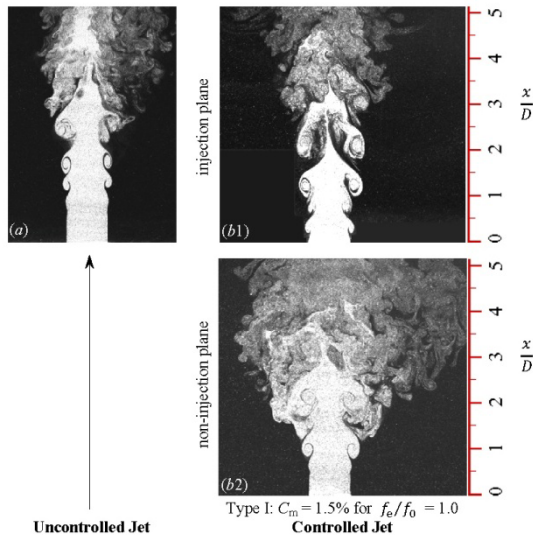


Figure 3. Photographs of typical flow structures from flow visualization. Flow is from the bottom up. (a) in the diametrical plane of the uncontrolled jet; (b1) in the injection plane and (b2) in the non-injection plane of the controlled jet (Type I: $C_m = 1.5\%$ for $f_e/f_0 = 1.0$)

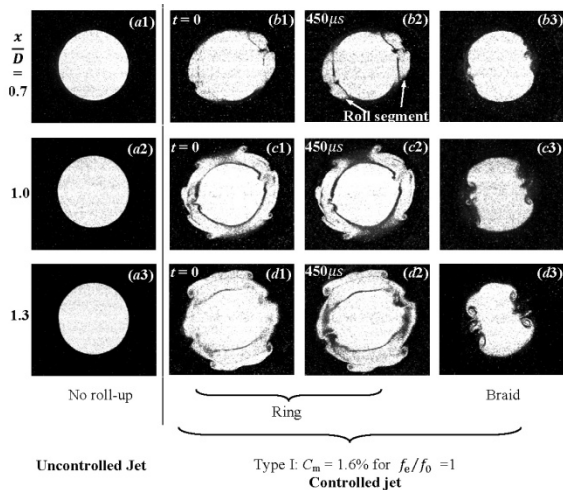


Figure 4. Photographs of flow visualization in the cross-sectional planes of $x/D = 0.7, 1.0, 1.3$. Flow is outward: (a1) $x/D = 0.7$, (a2) 1.0 and (a3) 1.3 of the uncontrolled jet; (b1-b3) $x/D = 0.7$, (c1-c3) 1.0 and (d1-d3) 1.3 of the controlled jet (Type I: $C_m = 1.6\%$ for $f_e/f_0 = 1.0$).

Two pairs of counter-rotating streamwise vortices are generated, following the rollup of roll segments about the injection plane. At $x/D = 0.7$, the cross section in the braid (figure 4b3) displays a profound distortion; two indentations occur under the influence of earlier rollup near the injection plane (figures 4b1 and 4b2). With increasing x/D , two pairs of counter-rotating streamwise vortices occur, simultaneously in the braid region and on the outer side of the ring vortex (figures 4c1, 4c2 and 4c3). Interestingly, their azimuthal locations all coincide well with the connecting

regions of the four roll segments. The counter-rotating vortex pair has an 'outflow' sense of rotation so that fluid in the jet core region may be ejected out into ambient fluid. The formation, including initial evolution, of the streamwise vortex pairs occurs at azimuthally fixed locations. The rotational senses of the streamwise vortices are opposite to the cases of steady microjets [5] and tabs [6], which all produced streamwise vortex pairs with an initial 'in-flow' sense such that ambient fluid is brought into the core region.

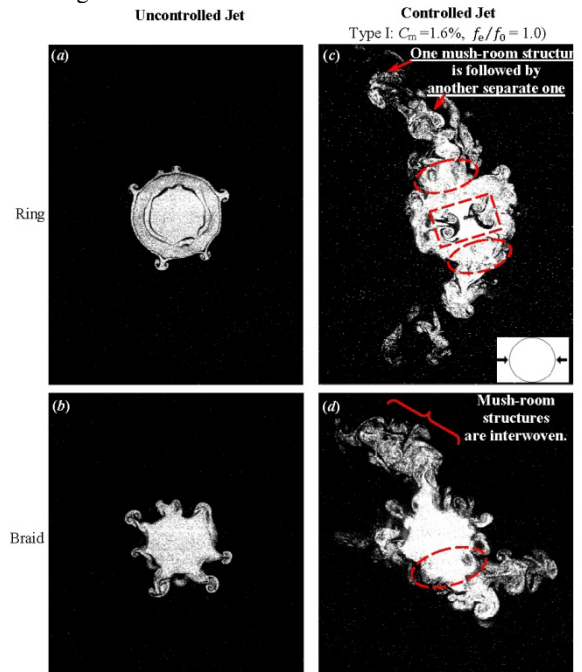


Figure 5. Photographs of flow visualization in the cross-sectional planes at $x/D = 3.0$.

The extraordinarily strong mixing, observed in the controlled jet of Type I (figure 3b2), is linked to a number of mushroom-like streamwise structures, which are sequentially 'tossed' out radially as seen in the non-injection plane. Figure 5 presents the images with and without control captured in a cross-sectional plane at $x/D = 3.0$. Both the azimuthal structure and the braid region are presented. The flow structures, be the azimuthal structure or the braid, are distinctly different between the uncontrolled and controlled jets. At $x/D = 3.0$ mushroom-like structures in the uncontrolled jet are evident in both the ring vortex and the braid region (figures 5a and 5b). These mushroom-like structures are characterized by counter-rotating streamwise vortex pairs of the 'out-flow' type, and are distributed azimuthally. Liepmann & Gharib [3] pointed out that, once formed, the mushroom-like structure first moved outward into the jet low-speed side due to self-induction and then went through the induced velocity field of the ring vortex. They were stretched in the braid region and re-entrained upstream into the adjacent ring vortex. This is why the streamwise structures generated are also observed in the ring vortex region. It is worth mentioning that the streamwise structures generated in the uncontrolled jet experience only one single 'generation' all the way to the end of the potential core. However, as shown in figure 5(c-d), in the controlled jet a number of mushroom-like structures are sequentially 'tossed' out along the radial direction in the non-injection plane. One may surmise that there could be several 'generations' of the streamwise structures generated under control. Often, one pair of mushroom-like counter-rotating structures follows another separate pair, as marked in figure 5(c). Sometimes, one mushroom-like structure is alternately interwoven with another, as marked in figure 5(d). This is accompanied by a strong ejection of jet core fluid, resulting in

greatly enhanced jet mixing. The formation of ‘tossed-out’ mushroom-like structures may be attributed to the presence of the azimuthally fixed streamwise vortex pairs of the ‘out-flow’ type in the controlled jet. Their presence tips the balance between the inward and outward inductions in the uncontrolled jet, resulting in a predominance of the radial outward induction. As a consequence, the mushroom-like structures are tossed out from the jet core region.

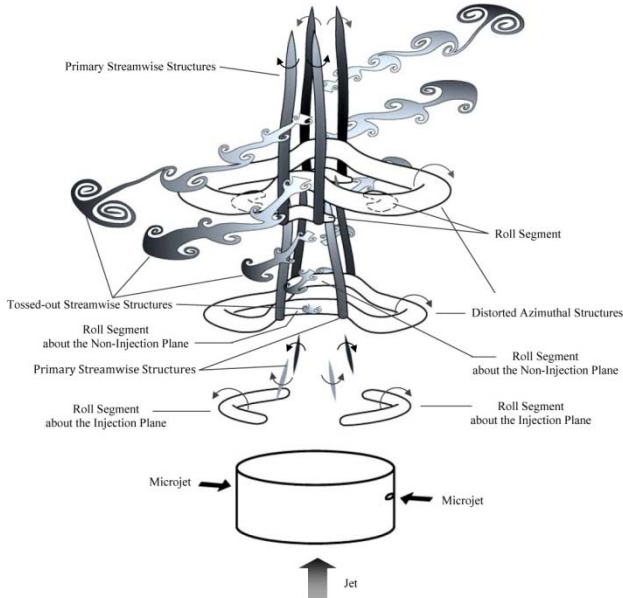


Figure 6. Conceptual model of the flow structure under the perturbation of two unsteady microjets.

A conceptual model is proposed based on the present experimental data for the jet flow structure under the excitation of two radial periodic microjets, as schematically shown in figure 6. The injected pulsed microjets cause the early rollup of the shear layer about the injection plane, and at the same time break the azimuthal symmetry in the braid region. The asymmetry causes the azimuthal vorticity in the braid region to be tilted, enhancing greatly the streamwise component of vorticity. Immediately downstream, two roll segments are formed about the non-injection plane and join the two roll segments about the injection plane with the reoriented ends for each segment. As such, a distorted azimuthal structure is formed. Then, the normal strain field in the braid region stretches the streamwise vorticity to form rapidly azimuthally fixed streamwise vortices of ‘out-flow’ type. The upstream end of a streamwise vortex is superposed upon the outer side of reoriented segments of the immediately upstream azimuthal structure. In contrast, the downstream parts stretch towards the inner side of the following azimuthal structure. Due to the braid instability, the mushroom-like structures are sequentially ‘tossed out’ along the non-injection plane, one pair after another, under the outward induction of streamwise vortex pairs. At the same time, in the injection plane a short roll segment is running towards the inner side of the distorted azimuthal vortex, entraining ambient fluid into the jet core region.

Conclusions

Experimental investigation has been conducted on the active control of a turbulent round jet ($Re_D = 8000$) using two radial unsteady microjets. Two control parameters are examined, i.e. C_m and f_e/f_0 . The effects of C_m on the control performance can be divided into Types I, II and III, in terms of required C_m and achievable K . The maximum K of Type I is about 8 times that in the uncontrolled jet. C_m required to achieve the maximum K is merely one third of its counterpart of steady microjets,

demonstrating high control efficiency in Type I. The flow physics of Type I were closely examined in the injection (x, y) plane, non-injection (x, z) plane, and eight cross-sectional (y, z) planes over $x/D = 0.45$ to 5.0 using hot-wire and flow-visualization techniques.

A conceptual model is proposed for the flow structure under the control of Type I, which is distinct from those under the control of tabs and steady microjets. The local microjet perturbation results in the early rollup of azimuthal roll segments about the injection plane, causing the cross section of the braid to deform. As a result, two pairs of azimuthally fixed streamwise vortices with an ‘out-flow’ sense of rotation are generated about the non-injection plane, stretching upstream and downstream between the outer side of the azimuthal vortex and the inner side of the following one. Under the influence of outward induction of azimuthally fixed streamwise vortices, the braid instability is amplified to generate sequentially the mushroom-like counter-rotating streamwise structures, which are ejected along the radial direction in the non-injection plane, one after another. Near the injection plane, a short roll segment catches up with the contorted azimuthal vortex without pairing but breaks down rapidly. This motion produces a strong entrainment of ambient fluid into the jet core, in distinct contrast with the significant spread about the non-injection plane.

Acknowledgments

YZ wishes to acknowledge support given to him from Research Grants Council of HKSAR through grant GRF 531912 and from Shenzhen City Government through grant JCYJ20120613134811717.

References

- [1] Davis, M. R., Variable Control of Jet Decay, *AIAA J.*, **20**(5), 1982, 606-609.
- [2] Henderson, B., Fifty Years of Fluidic Injection for Jet Noise Reduction, *International J. Aeroacoustics*, **9**, 2010, 91-122.
- [3] Liepmann, D. & Gharib, M., The role of streamwise vorticity in the near-field entrainment of round jets, *J. Fluid Mech.* **245**, 1992, 643-668.
- [4] Mi, J., Nathan, G. J. & Luxton, R. E., Centreline Mixing Characteristics of Jets from Nine Differently Shaped Nozzles, *Exp. Fluids*, **28**, 2000, 93-94.
- [5] New, T. H. & Tay, W. L., Effects of cross-stream radial injections on a round jet. *J. Turbul.* **7**, 2006, 1-20.
- [6] Reeder, M. F. & Samimy, M., The evolution of a jet with vortex-generating tabs: Real-time visualization and quantitative measurements, *J. Fluid Mech.* **311**, 1996, 73-118.
- [7] Seidel, J. F., Pappart, C., New, T. H. & Tsai, H. M., Effects of Multiple Radial Blowing around a Circular Jet, in *43th AIAA Aerosp. Sci. Meet.*, American Institute for Aeronautics and Astronautics, 2005, *Pap.* 2005-0866.
- [8] Zhang, P., Zhou, Y. & Alam, M. M., Active Control of a Round Jet Using Two Unsteady Microjets, in *18th Australasian Fluid Mechanics Conference*, Launceston, Australia, 3 – 7 December, 2012, *Paper No.* 53.
- [9] Zhou, Y., Du, C., Mi, J. & Wang, X. W., Turbulent Round Jet Control Using Two Steady Minijets, *AIAA J.*, **50**(3), 2012, 736-740.